CrossMark

RESEARCH PAPER

Effect of Material Anisotropy on Delamination Damage in Adhesive Bonded Lap Shear Joints Made with Curved Laminated FRP Composite Panels

S. K. Parida[1] · A. K. Pradhan[2]

Abstract This paper deals with mixed mode fracture behaviour of embedded delaminations in lap shear joints (LSJs) made with curved laminated FRP composite panels under uniform applied extension. The delaminations are presumed to be pre-existed at the interface of the first and second plies of the strap adherend of the LSJ at a location more prone to failure as per Tsai–Wü failure criterion. Three-dimensional nonlinear finite element analyses of several LSJs have been carried out using contact and multi-point constraint (MPC) elements. Progressive growth of embedded delamination has been simulated by sequential release of the MPC elements. Strain energy release rate (SERR), being an indicative parameter, has been computed using virtual crack closure technique for assessment of structural integrity of the LSJs. The inter-laminar stresses and the three individual modes of the SERR in the vicinity of either end of the delamination front are found to be much different from each other indicating dissimilar rates of growth of delamination. The degree of anisotropy of the materials of the curved adherend panels influences the inter-laminar stresses and therefore the SERRs in the vicinity of the delamination fronts. Thus, a choice can be made in favour of use of some particular type of FRP composite materials wherein the SERR values would be less, thereby enhancing the overall strength and structural integrity of the LSJs. Here in this paper, it has been found that glass/epoxy material is better suited either to prevent or slow down the delamination propagation if the strength requirement is met.

1 Introduction

Joining of curved fibre reinforced plastic (FRP) composite panels is usually carried out with adhesive bonding in aerospace structures. Adhesively bonded lap shear joint (LSJ) is one of many such examples. Advantages of adhesively bonded joints over mechanically fastened joints are the simplicity in design, reduced stress concentrations because of elimination of holes and cut-outs, savings in weight and cost. Most often these FRP laminates are found to have delaminations/debonding at inter-laminar locations because of inclusion of air bubbles, impurities, etc. during their manufacturing processes. Initially, intact laminated panels may also develop delamination while in service or due to low-velocity impact such as drop of hammers. Delaminations in FRP composite panels cause large drop in strength, stiffness and the load-carrying capacity. Such damages once started, the growing changes in the stress distributions may induce delaminations at several other locations. This may lead to final catastrophic failure of the total structure. In this paper, three-dimensional nonlinear finite element analyses (FEA) of LSJs made with curved FRP composite panels have been carried out. In delamination studies of lap joints made with FRP composite adherends, inter-laminar peel and shear stresses and strain

✉ S. K. Parida
sambitparida@gmail.com

A. K. Pradhan
akpradhan@iitbbs.ac.in

[1] School of Mechanical Engineering, KIIT University, Bhubaneswar 751024, India

[2] School of Mechanical Sciences, IIT, Bhubaneswar 751013, India

energy release rate (SERR) components are important parameter for onset and growth of pre-existing delaminations (Czarnocki 2000; Das 2010; Das and Pradhan 2013; and Yang et al. 2003). Earliest among the reported lap joint theories is by Volkersen (1938) where he has ignored the tearing stresses in adhesive layer and the stress variation along the thickness of adhesive used to join the adherends. In a subsequent two-dimensional theoretical analysis of lap joint by Goland and Reissner (1944), few short comings of Volkersen's theory like deformation of adherends due to bending and tearing stress in adhesives are taken into consideration. Results of these theories demonstrate the existence of complicated stress variations in the joint. Later pre-existed adhesion failure in between the lap and strap adherends of single lap joint made with flat FRP composites has been analysed (Lai et al. 1996 and Tong 1996) using beam theory. Hart-Smith (1973) and Adams (1989) are amongst those who first employed FEA to determine stress fields in adhesively bonded joints. The investigations on the influence of local geometrical changes like the adhesive spew fillets at the overlap ends of the joints by Adams and Haris (1987) and Tsai et al. (1998) are some of the initial classical researches carried out using 2D FEA. The research papers of Panigrahi and Pradhan (2009), Pradhan and Parida (2012) and Panigrahi (2013) give a detailed account of a good number of pertinent literatures over a wide range of delamination related issues in various lap joints made with FRP composite structures. Tay's (2003) review paper gives an overview of methods used over a period from 1990 to 2001 for analyses of adhesive bonded joints. Nassar et al. (2012) have recently published a research paper on the effect of damage on strength and integrity of adhesively bonded single lap joint made with thick composite laminates. Chen et al. (2011) in their paper recommended the use of energy-based fracture criterion for the initiation and propagation of crack in the single lap joint (SLJ) made with metallic adherends. Karachalios et al. (2013) have experimentally demonstrated the linear and nonlinear variations of effect of shape and size of adhesion failure area on strength of the SLJ made with different grades of adherend and adhesives (both brittle and ductile). Progressive damage and failure propagation pattern in fibres and matrix of a laminated FRP composite plate having a through hole under tensile load have been analysed by Zhang and Zhao (2012) using FE method. They have presented the matrix cracking and fibre breakage phenomena and subsequent failure propagation around the hole in the FRP composite plate. Cheuk and Tong (2002) have done plane strain FE analyses of LSJ having pre-embedded delamination. They have also found out experimentally the effect of different delamination sizes on the strength of joint till complete failure. The effect of ratio of axial to transverse elastic stiffness on the stress

concentration around holes in composite plates has been demonstrated by Pradhan (1982) using two-dimensional FE analyses. Tian and Fu (2011) have reported a nonlinear analysis of delaminated composite plate having interfacial delamination under transverse load using higher-order shear deformation theory. The numerical results of the analyses show that the transverse normal stress should be carefully evaluated near the delamination front. The level of transverse normal stress is abruptly high near the delamination front due material discontinuities when pulling load is applied and the in-plane shear stress becomes dominant when the laminate is subjected to transverse pushing load. A newer method to accurately model the complex shape of the delamination in laminated composite plates and panels using non-uniform rational b-splines has been proposed by Nguyen et al. (2014a, b). It is also reported to generate interface elements in the delamination region which can have cohesive zone material properties along the complex contour of the delamination created by using non-uniform rational b-spline (NURB) in the modelling phase (Nguyen et al. 2014a, b; Dimitri et al. 2014). An effective simulation of delamination in skin stiffener has been presented by Dávila et al. (2008) using shell and zero-thickness cohesive element to predict the mixed mode propagation in bend test. They have also demonstrated modelling delamination of thick shells by stacking several shell elements along with cohesive elements. A numerical study on skin–stringer debonding growth in stiffened composite panels has been carried out by Riccio et al. (2015) to model delamination propagation in stiffened composite panel in the presence of skin–stringer partial separation. They have discussed methods to overcome the mesh size, time increment dependency and the complexities associated with modelling circle-shaped delamination of the standard virtual crack closure technique (VCCT). Further, the methodology proposed by Riccio et al. (2016) is reported to be computationally inexpensive for delamination propagation studies in stiffened panel. Parida and Pradhan (2014) has recently published an article on the effect of size of the pre-embedded delamination on the inter-laminar stresses and SERR in the vicinity of delamination fronts present in the strap adherend of the LSJ made with flat FRP composite. They have recommended the use of 3D FE to capture the three-dimensional variation of inter-laminar stresses near the delamination fronts due to bending–twisting coupling. The simultaneous consideration of factors like material anisotropy, discontinuities due to delaminations, curved geometries, eccentric loading path in the analyses of LSJ makes the three-dimensional closed-form solution of the problem very complex. Hence, three-dimensional FE analyses of LSJs made with curved FRP adherends have to be carried out. Numerous papers have appeared in the

recent literature on the subject of delamination damage in laminated FRP composites, but very few have devoted to the studies on effect of design parameters like effect of degree of anisotropy of adherend materials on the delamination damage growth in LSJ made with curved FRP composite adherends. Since LSJs made with curved FRP adherends are widely used in the areas of aerospace industries, this puts forth a requirement of generation of new and additional research data for effective use of such joints. Various design parameters like length, width, thicknesses, radius of curvature, elastic stiffness ratios (E_z/E_r) and (E_z/G_{zr}) of adherend materials, loading type, eccentricity in loaded path, delamination locations and sizes affect the inter-laminar stress distributions and SERR in the vicinity of delamination fronts embedded in the LSJ made with FRP composite panels.

The objective of this paper is to analyse the effect of ratio of elastic stiffness (E_z/E_r) and (E_z/G_{zr}) of adherend materials on the inter-laminar stresses (σ_r, τ_{rz}, $\tau_{r\theta}$) and the evaluation of the three modes of SERR (G_I, G_{II} and G_{III}) in the vicinity of pre-embedded delaminations in between the first and second plies of strap adherend of the LSJs made with curved FRP composite panels under uniform applied in-plane extension using three-dimensional finite element methods. Effect of delamination sizes on SERR at both the delamination fronts for three different adherend materials with varying degrees of anisotropies has also been discussed.

2 Configuration and Loading of the Adhesively Bonded LSJ Made with Curved Laminated FRP Composite Panels Containing Pre-embedded Delamination

The lengths of lap and strap adherends, width, radius of curvature, loading and boundary conditions of the LSJ made with curved adherend panels are shown in Fig. 1. All the degrees of freedoms in the stiffened end of the LSJ are restrained, and the un-stiffened end of the LSJ is loaded with uniform applied displacement of $\Delta = 0.1$ mm. The inner radius of curvature of the curved strap adherend is $R = 71.6$ mm and the shallowness angle of the curved panel $\theta = 20°$ such that the width (w) of the strap adherend is 25 mm. Three different adherend materials namely glass/epoxy (Gl/E), carbon/epoxy (C/E) and boron/epoxy (B/E) have been used. The lap and the strap adherends are made of plain woven pre-pregs, and the engineering material properties of each ply of adherend materials are given in Table 1 (Das 2010; Pradhan and Parida 2012). The degree of anisotropy of an anisotropic material is defined with parameters such as the ratio of E_z/E_r or E_z/G_{zr}. The relative comparison of degree of anisotropy of FRP composite

materials of the adherends of the LSJs used in the analyses is shown in Fig. 2. Each curved adherend panel is made of eight plies laid along 0°, i.e. z direction. Film adhesive FM 300-K of Cytek make has been used to join the lap and the strap curved adherends, whose isotropic material properties are given in Table 2. The thickness of each ply and adhesive layer is 0.125 mm. Delaminations of various lengths $2a = 2, 4, 6, 8, 10$ mm are presumed to be pre-embedded between the first and second plies of the curved strap adherend. AB and CD are the two fronts of the delamination, the former being situated under the overlap region below the lap adherend, while the later is located outside the overlap region.

An initial analysis has shown that any pre-existed delamination due to manufacturing defect or otherwise induced during service loading in the strap adherend invariably shows a grater loss of structural integrity of the LSJ than that of a pre-existed delamination in the lap adherend. In this research, therefore, a pre-embedded delamination has been presumed to be pre-existed (be pre-embedded) at the interface of the first and second plies of the curved strap adherend.

## 3 FE Modelling and Simulation of Pre-embedded Delamination in the LSJ

Three-dimensional FE modelling of the LSJ containing pre-embedded delamination has been carried out by using eight-noded layered brick SOLID 185 elements of ANSYS 14.5 to model the curved lap and the strap adherends and normal eight-noded volume SOLID 185 elements to discretize the isotropic adhesive layer between the two adherend panels. The mesh density of the finite elements has been increased near the delamination fronts (shown in Fig. 3) to ensure the convergence of the solution as per the guidelines provided in reference by Tay et al. (1999) and Raju et al. (1988). Accordingly, element size equal to one-fourth of each ply thickness has been used near the delamination fronts. Sub-laminate modelling techniques have been used to model the embedded delamination in between the first and second plies of the strap adherend (Fig. 4). At the delaminated interface, duplicate nodes have been provided between the sub-laminates. In the un-delaminated region, corresponding nodes of the two sub-laminates are constrained by using multi-point constraint (MPC) elements so that continuity conditions prevail. By sequentially releasing the constraints of these MPC elements, progressive delamination propagation is made to occur. MPC elements on the delamination fronts will give the nodal forces required to hold the delaminated surfaces together which is required to be used to calculate the SERRs given in Eqs. (4–6). As the LSJ undergoes an
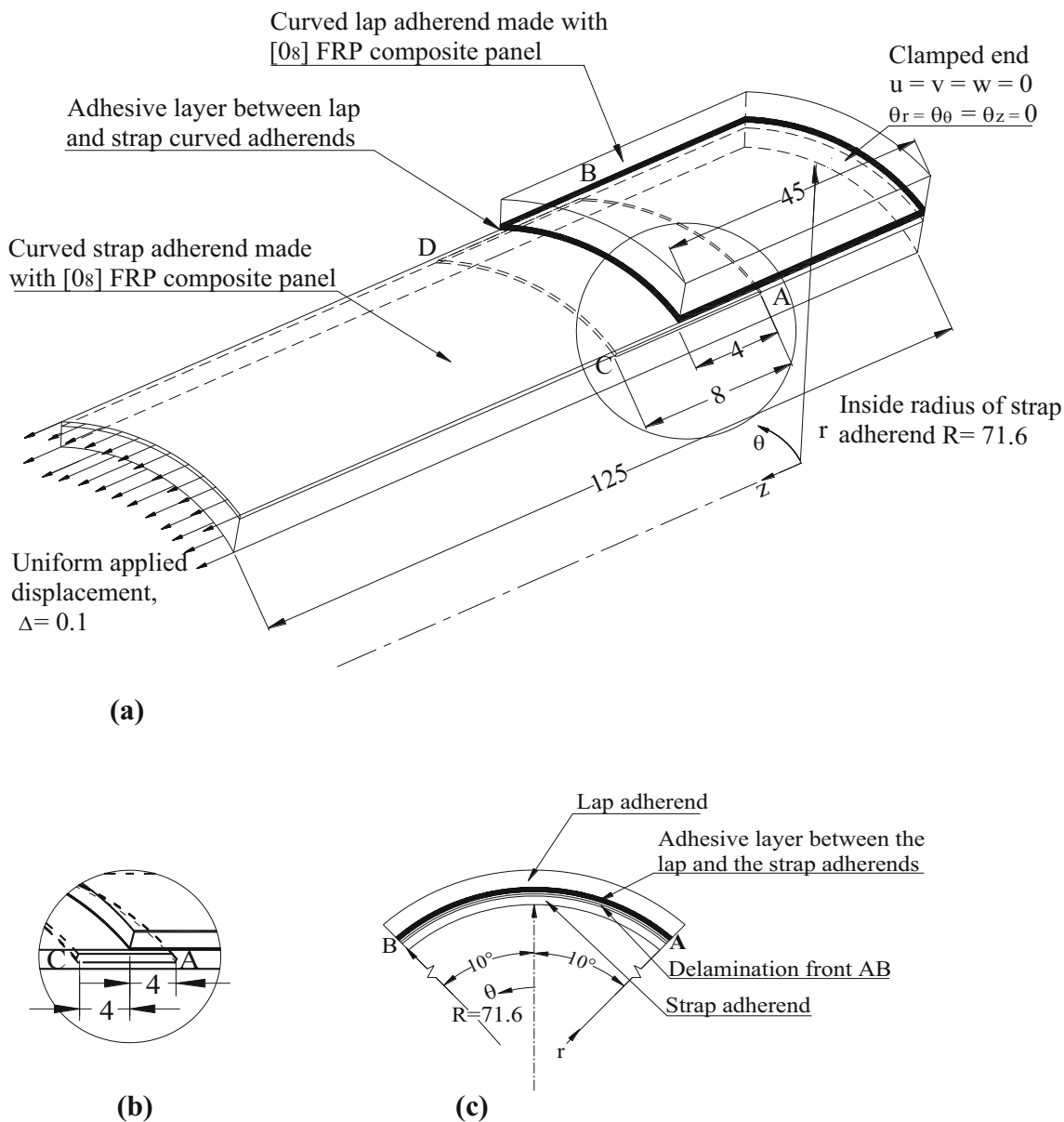
Fig. 1 LSJ with delamination of 8 mm length pre-embedded at the interface of first and second plies of the curved strap FRP composite adherend (all dimensions are in millimetre). **a** Configuration and loading of the LSJ. **b** Zoomed view X. **c** Two-dimensional transversal view of LSJ

Table 1 Material properties of FRP composite adherends used in LSJ with varying degree of anisotropy (Das 2010; Pradhan and Parida 2012)

| Material	Young's moduli			Poisson's ratio			G_{zr} (GPa)	Parameter defining degree of anisotropy	
	E_z (GPa)	E_r (GPa)	E_θ (GPa)	v_{rz}	$v_{\theta z}$	$v_{r\theta}$		E_z/E_r	E_z/G_{zr}
Gl/E [0_8]	54.85	18.28	18.28	0.08	0.027	0.38	9.14	3.00	6.01
B/E [0_8]	210.98	21.00	21.00	0.04	0.025	0.38	7.03	10.00	30.01
C/E [0_8]	181.00	10.30	10.30	0.01	0.010	0.30	7.17	17.57	25.24
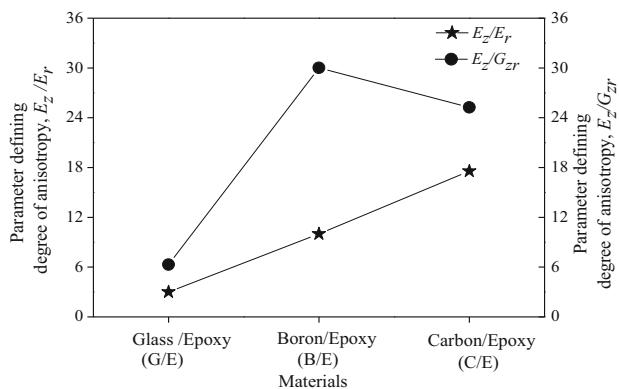
Fig. 2 Comparative degree of anisotropy of FRP composite materials used in the analyses of the LSJs

Table 2 Mechanical properties of FM 300-K film adhesive (Cheuk and Tong 2002)

Young's modulus [E (GPa)]	2.40
Poisson's ratio (v)	0.32
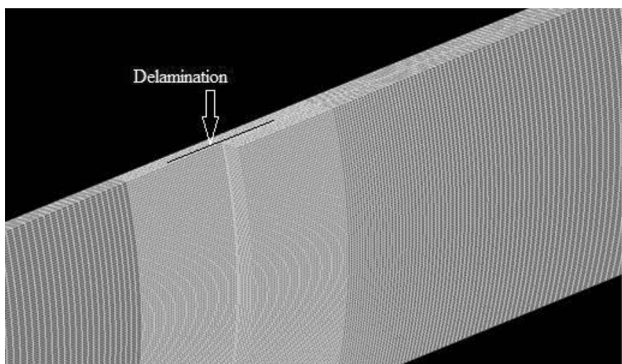
Fig. 3 FE mesh of the LSJ having pre-embedded delamination
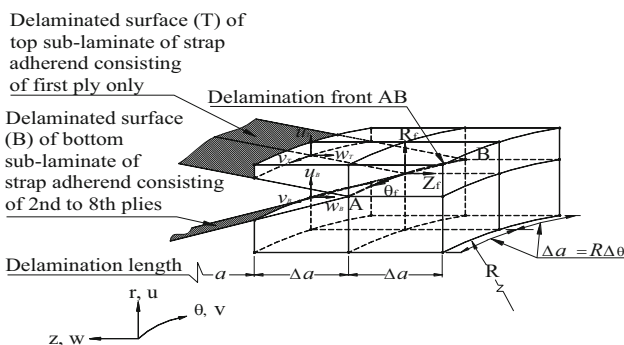
Fig. 4 Schematic of FE model in the vicinity of curved delamination front AB present in the LSJ made with curved composite panels for the computation of SERRs by MCCI and VCCT methods

apparent off-axis (eccentric) loading path, interpenetration of the delaminated surfaces may likely to occur. To prevent this, over the delaminated region, the corresponding nodes of the top and the bottom delaminated surfaces have been connected by means of three-dimensional two-noded contact elements (CONTA 178).

The contact elements become active only when the two delaminated surfaces come into contact, and thus, these elements between the layers prevent the interpenetration of the delaminated surfaces. The inter-laminar stresses are calculated from these nonlinear three-dimensional finite element analyses for the LSJ made with three different adherend materials (Table 1) of varying material anisotropies. The non-linearity in the analyses is due to eccentric loading path, curved geometry of the adherends, contact non-linearity and material anisotropy.

In the study of delamination onset and growth behaviour in FRP composite bonded joints, the SERR criterion is considered to be a very useful parameter for predicting the damage growth (Finn and Springer 1993; Wang and Vu-Khanh 1995; and Panigrahi and Pradhan 2009). Not only it is based on sound energy balance principle related to work done in new crack face generation, but also mixed mode inter-laminar delamination progression can be separated into individual fracture modes which can be suitably compared with experimental observations of critical SERRs. The delamination-induced damages in FRP composite materials are characterized by three modes of SERR, i.e. modes I, II and III, respectively, as have also been emphasized (Dattaguru et al. 1994; Wang and Raju 1996; Panigrahi and Pradhan 2007). The three components of SERR G_I, G_{II} and G_{III} can be computed by modified crack closure integral (MCCI) method developed by Irwin (1957) and subsequently emphasized by Rybicki and Kanninen (1977). In SERR method of delamination propagation studies, the computation of values of the stresses exactly at the delamination fronts is not being much emphasized. The stresses and the displacements are evaluated over the incremental delaminated areas. These values are used in the computation of G_I, G_{II} and G_{III}. Further, it is not required to use a very refined mesh in the region (Tay et al. 1999). They have discussed in details the adequacy of the local near-tip mesh discretization schemes. They have also warned that an extreme fine mesh could result in non-convergence or create oscillatory stress fields. Rice (1988) has suggested to use element size of characteristic length equal to 0.25–0.5 of the ply thickness to evaluate correctly the SERR components. Another advantage of this method is that it is not very sensitive to mesh design as indicated by Raju et al. (1988), Tay et al. (1999).

3.1 MCCI Method of Computation of SERR

Referring to Fig. 4, the SERRs with respect to the three modes of fracture I, II and III are evaluated as follows:

$$G_{\mathrm{I}} = \lim_{\Delta A \to 0} \frac{1}{2\Delta A} \int_{a}^{a+\Delta a} \int_{-\frac{r\Delta\theta}{2}}^{\frac{r\Delta\theta}{2}} \sigma_r(\theta, z)$$
$$\times \left[u_{\mathrm{T}}(\theta, (z - \Delta a)) - u_{\mathrm{B}}(\theta, (z - \Delta a))\right] r \, \mathrm{d}\theta \, \mathrm{d}z \qquad (1)$$

$$G_{\mathrm{II}} = \lim_{\Delta A \to 0} \frac{1}{2\Delta A} \int_{a}^{a+\Delta a} \int_{-\frac{r\Delta\theta}{2}}^{\frac{r\Delta\theta}{2}} \tau_{rz}(\theta, z)$$
$$\times \left[w_{\mathrm{T}}(\theta, (z - \Delta a)) - w_{\mathrm{B}}(\theta, (z - \Delta a))\right] r \, \mathrm{d}\theta \, \mathrm{d}z \qquad (2)$$

$$G_{\mathrm{III}} = \lim_{\Delta A \to 0} \frac{1}{2\Delta A} \int_{a}^{a+\Delta a} \int_{-\frac{r\Delta\theta}{2}}^{\frac{r\Delta\theta}{2}} \tau_{r\theta}(\theta, z)$$
$$\times \left[v_{\mathrm{T}}(\theta, (z - \Delta a)) - v_{\mathrm{B}}(\theta, (z - \Delta a))\right] r \, \mathrm{d}\theta \, \mathrm{d}z \qquad (3)$$

where subscripts T and B represent the top and bottom delaminated surfaces, respectively. The embedded delamination length is denoted by 'a' and 'Δa' is the virtual delamination length caused due to the external loading. Here, $[u_{\mathrm{T}}, v_{\mathrm{T}}, w_{\mathrm{T}}]$ and $[u_{\mathrm{B}}, v_{\mathrm{B}}, w_{\mathrm{B}}]$ represent the displacements corresponding to the nodes at the top and the bottom delaminated surfaces, respectively, behind the delamination front, and $\sigma_r(\theta, z)$, $\tau_{rz}(\theta, z)$ and $\tau_{r\theta}(\theta, z)$ are the stresses required to close the delaminated surfaces. $\Delta A(=\Delta a \times R\Delta\theta)$ is the area virtually considered to be closed while evaluating the SERR components by the crack closure integral method.

3.2 VCCT Implementation for Computation of SERR

In the Rybicki and Kanninen (1977) method of VCCT implementation in the FE analysis, stress-based Eqs. (1–3) take the form of simple multiplication of corresponding nodal forces at the FE nodes on the damage plane ahead of the delamination failure front and damage face displacements behind it (Eqs. 4–6). To implement this, (a) the FE mesh should be symmetric on the damage plane, (b) the element size should be small, and (c) the normality of the FE mesh should be maintained near the damage front. As per the VCCT procedure, the components of SERR for the LSJ with curved panels and containing embedded delamination are calculated as follows:

$$G_{\mathrm{I}} = \frac{1}{2\Delta A} R_{\mathrm{f}}(u_{\mathrm{T}} - u_{\mathrm{B}}) \qquad (4)$$

$$G_{\mathrm{II}} = \frac{1}{2\Delta A} Z_{\mathrm{f}}(w_{\mathrm{T}} - w_{\mathrm{B}}) \qquad (5)$$

$$G_{\mathrm{III}} = \frac{1}{2\Delta A} \theta_{\mathrm{f}}(v_{\mathrm{T}} - v_{\mathrm{B}}) \qquad (6)$$

where $\Delta A(=\Delta a \times R\Delta\theta)$ is the area virtually closed and R_{f}, Z_{f} and θ_{f} denote the opening, sliding and tearing forces, respectively, which are required to hold the nodes at the delamination damage front together to prevent it from growth and subsequent propagation. The displacements corresponding to the nodes at the top and the bottom delaminated surfaces, respectively, are represented by $[u_{\mathrm{T}}, v_{\mathrm{T}}, w_{\mathrm{T}}]$ and $[u_{\mathrm{B}}, v_{\mathrm{B}}, w_{\mathrm{B}}]$. The use of MPC elements at the delamination fronts enables computation of constraint forces R_{f}, Z_{f} and θ_{f}.

3.3 Advantage of VCCT Method Over MCCI for Computation of SERR

The values of three components of SERR G_{I}, G_{II} and G_{III} computed using numerical integration vide Eqs. (1–3) in MCCI and Eqs. (4–6) of VCCT method work out to be same as established by Rybicki and Kanninen (1977). Thus, both the methods are equivalent. The practical difficulties associated with the use of MCCI method are the need for a very fine mesh. This encompasses the following difficulties:

- Generation of the model can be time-consuming.
- Analysis tends to be computationally expensive.
- Test for convergence studies is usually needed to verify that mesh is adequate, and these are in themselves cumbersome and time-consuming.
- Numerical integrations Eqs. (1–3) involving stress and displacement fields in the neighbourhood of delamination fonts may be difficult, whereas in VCCT method computation of SERR is much simpler through a direct multiplication of nodal forces of the MPC elements at the delamination front and nodal displacements of nodes at gap elements behind the delamination front.

The three components of SERR have been computed using VCCT method in the present analyses.

4 Results and Discussion

4.1 Influence of Material Anisotropy of Laminated FRP Composite Adherends on Inter-laminar Stresses Along Delamination Fronts AB and CD

Performance of FRP composite laminates is limited by their inherent weaker resistance to inter-laminar stresses. The inter-laminar stresses can cause delamination or debonding at the inter-laminar locations. Figure 5

Fig. 5 Deformation of the LSJ having delamination under load

Zoomed portion (A) of the delamination in LSJ under load
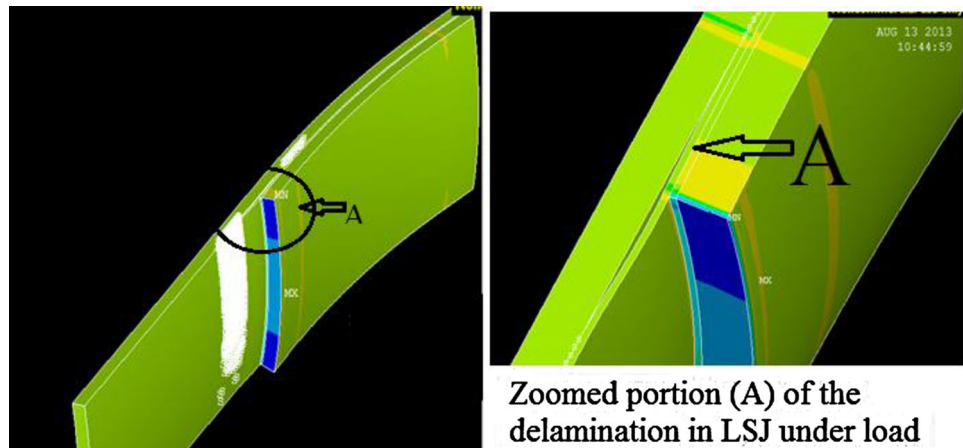
shows the deformed shape of the delaminated LSJ made with curved panel under uniform applied extension. The joint also bends due to eccentric loading path apart from getting delaminated. The variation of inter-laminar stresses due to anisotropy effects and their sizes in both the delamination fronts is discussed in this section. Variations in degree of anisotropy of the composite material also affect the stress distributions in the vicinity of the delamination fronts. Inter-laminar stresses can be reduced by choosing appropriate materials of the adherends. The peel stress (σ_r), shear stress (τ_{rz}) and cross-shear stress ($\tau_{r\theta}$) in the vicinity of delamination fronts AB and CD of a 8-mm-long and 25-mm-wide pre-embedded delamination in between the first and second plies of the strap adherend of the LSJ are shown in Figs. 6a–c and 7a–c, respectively, for [0_8] glass/epoxy (Gl/E), [0_8] boron/epoxy (B/E) and [0_8] carbon/epoxy (C/E) FRP composite materials. The variations of σ_r, τ_{rz} and $\tau_{r\theta}$ along delamination fronts AB and CD are shown with respect to the increase in degree of anisotropy E_z/E_r and E_z/G_{zr} of the adherend materials.

Salient observations are as follows:

- The magnitude of peel stress (σ_r) is minimum for the LSJ made with [0_8] Gl/E and is maximum for the [0_8] B/E material along the delamination front AB.
- Peel stress (σ_r) is not uniform along the delamination front AB. It is minimum at edges A and B.
- The peel stress (σ_r) in the delamination front CD is compressive in nature and varies with respect to varying anisotropy ratios E_z/E_r and E_z/G_{zr} of adherend materials (Fig. 7a). The compressive nature of peel stress in the delamination front CD excludes the chance of opening mode of failure. It is a beneficial point.
- The magnitude of shear stress (τ_{rz}) also increases with increase in degree of anisotropy in delamination fronts AB and CD.

- Magnitude of shear stress (τ_{rz}) is maximum at the edges and minimum at the central region in both the delamination fronts.

The non-uniform variation of inter-laminar stresses is due to the following reasons:

1. Mismatch of material properties, i.e. Young's modulus, Poison's ratio between the laminae and the coupling effects arising thereof.
2. Peel stresses (σ_r) in the delamination fronts AB and CD are due to the transverse deflection in radial direction arising from the eccentric loading path. At the free edges, peel stress (σ_r) is also developed from the moment equilibrium of forces involving cross-shear stresses ($\tau_{r\theta}$).
3. The cross-shear stress ($\tau_{r\theta}$) is developed to maintain equilibrium of forces resulted due to the normal stress (σ_θ). This is due to the Poison's effect as described in the literature Pagano and Pipes (1973).
4. Stress concentration occurs at delamination fronts due to discontinuities.
5. Geometrical non-linearity due to curvature of curved adherend also contributes to the non-uniform variation of inter-laminar stresses.
6. The degree of anisotropy significantly alters the magnitudes of inter-laminar stresses in delamination fronts AB and CD.

The combined effects of all the above factors make the state of stress in the vicinity of delamination front truly three-dimensional. The peak values of inter-laminar stresses along the delamination fronts AB and CD are shown with respect to increasing degree of anisotropy (E_z/E_r and E_z/G_{zr}) (Figs. 8, 9). It is found that LSJs made with B/E composite materials have higher values of inter-laminar stresses in both the delamination fronts. This is so due to higher coupling effect caused by higher values of E_z/G_{zr} by this material.

(a)

(b)

(c)
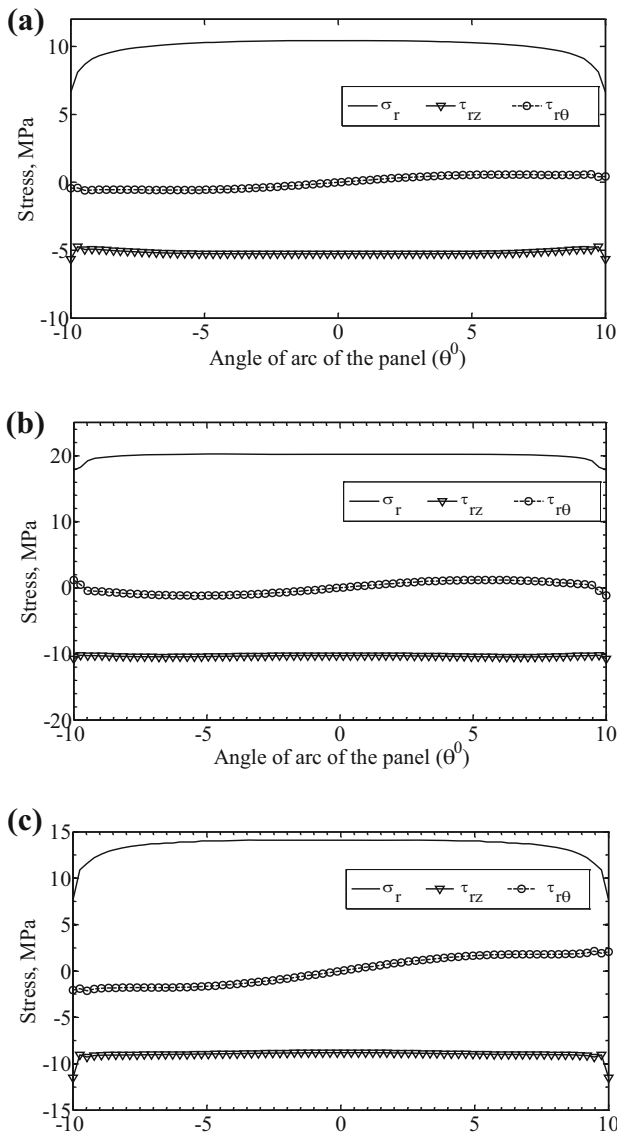
Fig. 6 Variations of inter-laminar stresses along the delamination front AB in LSJs made with Gl/E, B/E and C/E FRP composite adherend panels (delamination length $2a = 8$ mm and $w = 25$ mm). **a** [0_8] Glass/epoxy (Gl/E) adherends. **b** [0_8] Boron/epoxy (B/E) adherends. **c** [0_8] Carbon/epoxy (C/E) adherends

4.2 Influence of Material Anisotropy of Laminated FRP Composite Adherends on Variations of SERR Along Delamination Fronts AB and CD

In this section, the growth and propagation of embedded delamination are assessed using SERR method. Krüeger and O'Brien (2001), Kairouz and Mathews (1993) and Chakraborty and Pradhan (2002) have used SERR method as an appropriate parameter for evaluation of onset and growth of artificial damage present in laminated FRP composite structures. They have concluded that the

(a)

(b)

(c)
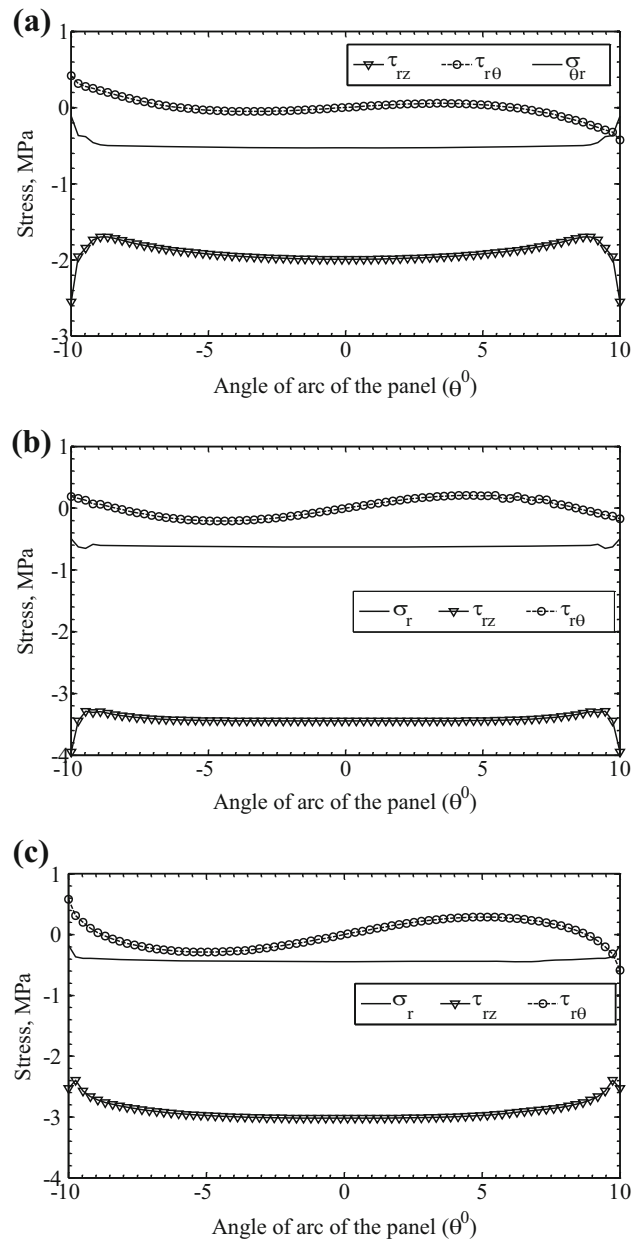
Fig. 7 Variations of inter-laminar stresses along the delamination front CD in LSJs made with Gl/E, B/E and C/E FRP composite adherend panels (delamination length $2a = 8$ mm and $w = 25$ mm). **a** [0_8] Glass/epoxy (Gl/E) adherends. **b** [0_8] Boron/epoxy (B/E) adherends. **c** [0_8] Carbon/epoxy (C/E) adherends

delamination fronts propagate from locations having higher SERR values. SERR variations along the delamination fronts AB and CD embedded in the curved strap adherend of the LSJ made with glass/epoxy, carbon/epoxy, boron/epoxy materials are shown in Figs. 10a–d and 11a–d, respectively. Salient observations are presented below.
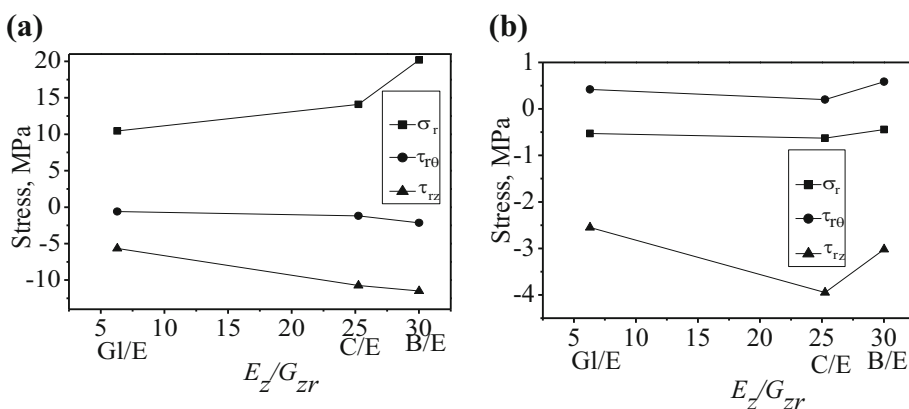
Mode I SERR (G_I) and mode II SERR (G_{II}) in the delamination front AB increase with the increase in degree of anisotropy (E_z/E_r and E_z/G_{zr}) of adherend materials. G_I

Fig. 8 Variations of peak values of inter-laminar stresses along delamination fronts with respect to degree of anisotropy E_z/E_r. **a** Delamination front AB. **b** Delamination front CD
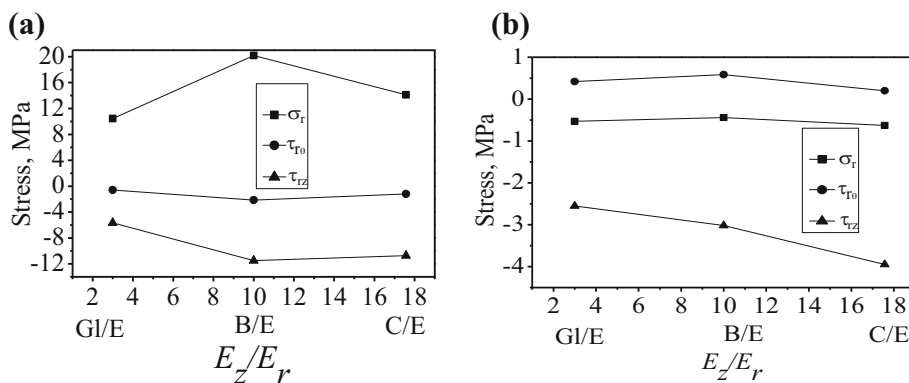
Fig. 9 Variations of peak values of inter-laminar stresses along delamination fronts with respect to degree of anisotropy E_z/G_{zr}. **a** Delamination front AB. **b** Delamination front CD


and G_{II} values are minimum for Gl/E material and maximum for B/E material. G_I is almost uniform excepting at the edges A and B. The variations of G_I follow the same trend of peel stress (σ_r) in the delamination front AB. Magnitude of mode III SERR (G_{III}) is much less and insignificant as compared to magnitudes of G_I and G_{II} in the delamination front AB. Mode I SERR (G_I) in the delamination front CD decreases with the increase in degree of anisotropy (E_z/E_r and E_z/G_{zr}) of adherend materials. As the peel stresses in the delamination front CD become increasingly compressive for materials having higher degree of anisotropy, the magnitude of G_I becomes less for materials having higher degree of anisotropy. Mode II SERR (G_{II}) values are higher than the corresponding G_I values and are seen to be the dominating mode of failure.

4.3 Influence of Delamination Size on Variations of SERR Along Delamination Fronts AB and CD

Figure 12a–d shows the effect of embedded delamination size on the variations of SERR in delamination fronts AB and CD, respectively, for the three different adherend materials (viz. Gl/E, B/E and C/E). G_I and G_{II} values

increase with increase in delamination lengths irrespective of the materials of the adherends in the delamination front AB. However, magnitude of G_I decreases with increase in delamination size as well as degree of anisotropy of adherend materials in the delamination front CD. This is due to compressive nature of the peel stresses for higher delamination sizes occurring due to bending effect. This reduces the chance of opening mode of failure along the delamination front CD for higher delamination lengths. The magnitude of G_{II} in the delamination front CD increases with increase in delamination sizes for all adherend materials. G_{III} values are much less as compared to G_I and G_{II} values in both the delamination fronts.

From the above observations, it is evident that delamination takes place in a mixed mode manner in both the fronts. G_I is the dominating mode of failure in the delamination front AB, whereas G_{II} mode of failure dominates in the delamination front CD. There is a general tendency of increase in total SERR (G_T) values with the increase in delamination lengths in the stiffened side of the LSJ (Fig. 13a). The delamination front propagates at a faster rate in the stiffened side than the delamination front outside the overlapped region as the total SERR (G_T) value of former is larger than the later (Fig. 13b). The evaluation of
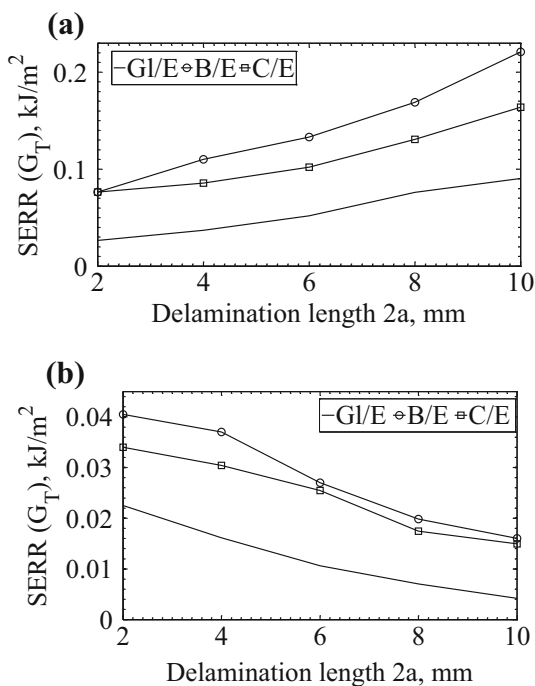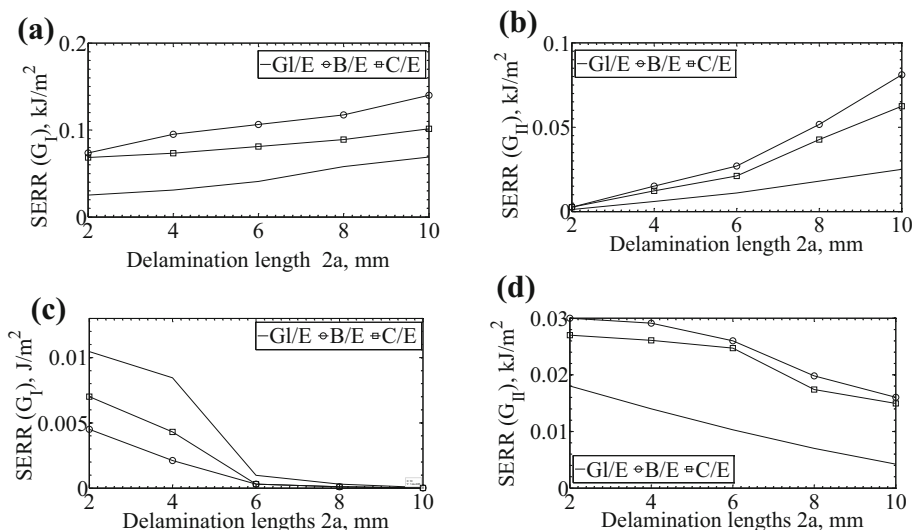
(a)

(b)

(c)

(d)
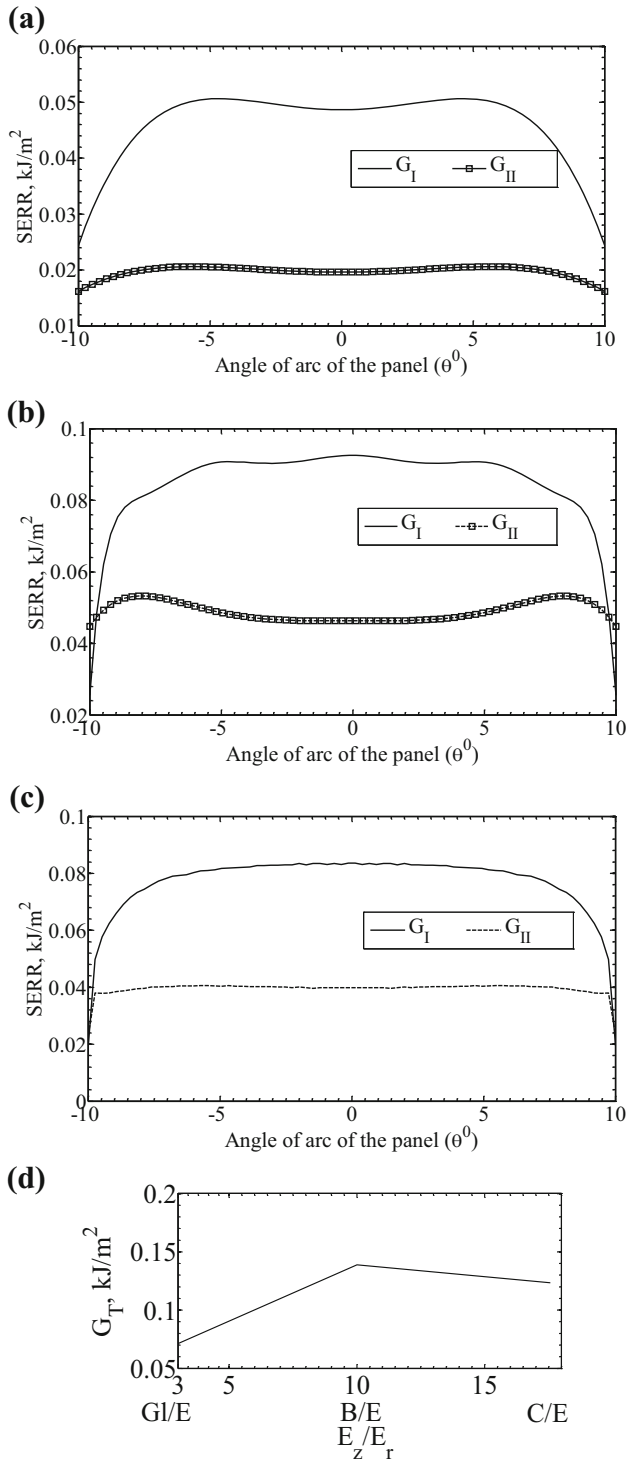
Fig. 10 Variations of mode I (G_I) and mode II (G_{II}) SERRs along the delamination front AB in LSJs made with Gl/E, C/E and (B/E) FRP composite adherend panels (delamination length $2a = 8$ mm and $w = 25$ mm). **a** $[0_8]$ Glass/epoxy (Gl/E). **b** $[0_8]$ Boron/epoxy (C/E). **c** $[0_8]$ Boron/epoxy (B/E) adherends. **d** Peak values of G_T along AB

SERR variations at both the delamination fronts with the increase in delaminations lengths would indicate how the LSJ gradually loses its structural integrity. This will be
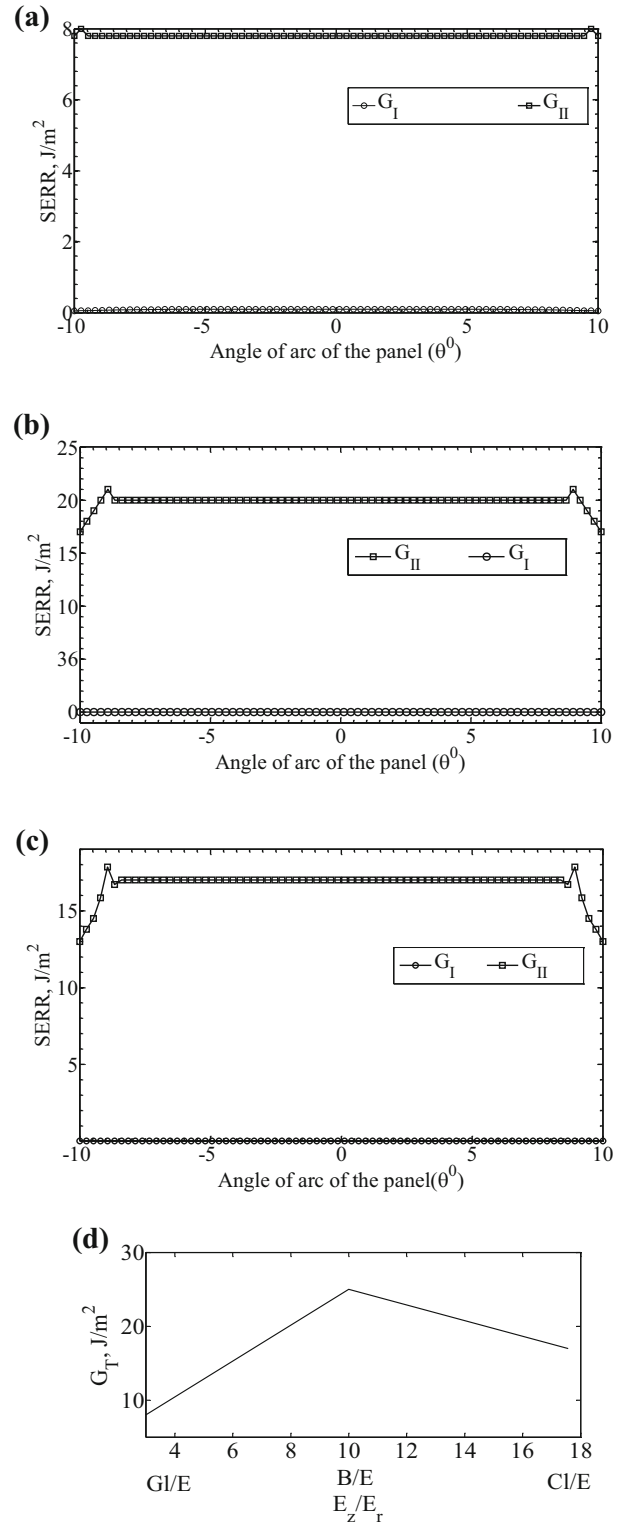
Fig. 11 Variations of mode I (G_I) and mode II (G_{II}) SERRs along the delamination front CD in LSJs made with Gl/E, C/E and (B/E) FRP composite adherend panels (delamination length $2a = 8$ mm and $w = 25$ mm). **a** $[0_8]$ Glass/epoxy (Gl/E) adherends. **b** $[0_8]$ Boron/epoxy (B/E) adherends. **c** $[0_8]$ Carbon/epoxy (C/E) adherends. **d** Peak values of G_T along CD

Fig. 12 Variations of SERR components for varying delamination sizes (2a = 2, 4, 6, 8, 10 mm) and degree of anisotropy. **a** G_I in delamination front AB. **b** G_{II} in delamination front AB. **c** G_I in delamination front CD. **d** G_{II} in delamination front CD

of G_I in the delamination fronts CD decrease with increase in degree of anisotropy (Fig. 12c, d). G_I is the dominating mode in delamination front AB whereas G_{II} is the dominating mode of failure in delamination front CD irrespective of the materials of adherends.

5 Conclusions

Three-dimensional nonlinear finite element analyses have been carried out to see the effect of increase in delamination size and the degree of anisotropy of adherend materials on three modes of SERR. The presence of embedded delaminations in the strap adherend of the LSJs made with curved FRP composite materials significantly influences the state of inter-laminar peel and shear stress distributions at the delamination fronts, therefore the SERR components. Salient observations are as follows:

- Peel and shear stress distributions in the vicinity of delamination fronts are found to be very complex in nature, demonstrating the existence of three-dimensional states of stress. Hence, simplified 2D plane stress analyses will lead to erroneous results. Three-dimensional FE analyses must be carried out for LSJs made with curved composite adherends containing embedded delaminations.
- Inter-laminar stresses near the edge and the central portion of the delamination fronts are seen to be significantly different demonstrating severe edge effects. The non-uniform variations of inter-laminar stresses are due to mismatch of Poisson's ratio and Young's moduli in the adjacent layers, curvature geometry, eccentric loading path and discontinuities due to the embedded delaminations.

Fig. 13 Variations of total SERR for varying delamination sizes (2a = 2, 4, 6, 8, 10 mm) for Gl/E, B/E and C/E adherend materials with different degree of anisotropy. **a** Delamination front AB. **b** Delamination front CD

similar to that as someone will observe while performing an actual experiment. So, in the absence of actual experiments, the present simulation procedure would serve as a very useful method to the designers.

There is an increasing trend in the values of G_I and G_{II} in the delamination front AB with the increase in the delamination size for all materials (Fig. 12a, b). This may be due to the increase in stress levels with the increase in degree of anisotropy of adherend materials. But, the values

- Inter-laminar stresses increase in the vicinity of the delamination fronts with the increase in degree of anisotropy of materials of the adherends.

- However, due to increase in degree of anisotropy of adherend materials the peel stress in the delamination front CD becomes more compressive indicating the reduced chance of mode I delamination propagation.

- Variations of individual modes of SERR show that the damage propagation takes place in a mixed mode manner. Further, the uneven variations of G_I, G_{II} and G_{III} will lead to non-self-similar delamination front propagation.

- SERR values are much different at the two delamination fronts. Since higher values of SERR indicate faster loss of structural integrity, the delamination damage is seen to propagate more rapidly from the delamination front trapped inside the overlap region.

References

Adams RD (1989) Strength predictions for lap joints, especially with composite adherends: a review. J Adhes 30:219–242

Adams RD, Haris JA (1987) The influence of local geometry on strength of adhesive joints. Int J Adhes Adhes 7:69–80

Chakraborty D, Pradhan B (2002) Fracture behaviour of FRP composite laminates with two interfacing embedded delaminations at the interface. J Reinf Plast Compos 21:681–698

Chen Z, Adams RD, Da Silva LFM (2011) Prediction of crack initiation and propagation of adhesive lap joints using an energy failure criterion. Eng Fract Mech 78:990–1007

Cheuk PT, Tong L (2002) Failure of adhesive bonded composite lap shear joints with embedded precrack. Compos Sci Technol 62:1079–1095

Czarnocki P (2000) Effect of reinforcement arrangement on distribution of G_I, G_{II}, G_{III} along fronts of circular delaminations in orthotropic composite plates. Eur J Struct Intergr Soc 27:49–60

Das RR (2010) Adhesion failure and delamination of bonded tubular joints made with laminated FRP composites and functionally graded materials. Ph.D. thesis, Indian Institute of Technology, Kharagpur, India

Das RR, Pradhan B (2013) Delamination damage analysis of laminated bonded tubular single lap joint made with fibre–reinforced polymer composite. Int J Damage Mech. doi:10.1177/1056789513513199

Dattaguru B, Ramamurthy TSV, Buchholz FG (1994) Finite element estimates of strain energy release rate components at the tip of an interface crack under mode I loading. Eng Fract Mech 49:451–463

Dávila CG, Camanho PP, Turon A (2008) Effective simulation of delamination in aeronautical structures using shells and cohesive elements. J Aircr 45:663–672

Dimitri R, De Lorenzis L, Wriggers P, Zavarise G (2014) Nurbs-and T-spline-based isogeometric cohesive zone modeling of interface debonding. Comput Mech 54:369–388

Finn SR, Springer GS (1993) Delaminations in composite plates under transverse static or impact loads: a model. Compos Struct 23:177–190

Goland M, Reissner E (1944) The stresses in cemented joints. ASME Trans J Appl Mech 7:A17–A27

Hart-Smith LS (1973) Adhesive bonded single lap joints. NASA-CR-112236. http://citeseerx.ist.psu.edu/viewdoc/download?doi=10.1.1.461.4731&rep=rep1&type=pdf. Accessed 15 Mar 2016

Irwin GR (1957) Analysis of stresses and strains near the end of the crack traversing in a plate. ASME Trans J Appl Mech 24:361–364

Kairouz KC, Mathews FL (1993) Strength and failure modes of bonded single lap joints between cross-ply adherends. Composites 24:475–484

Karachalios EF, Adams RD, Da Silva LFM (2013) Strength of single lap joints with artificial defects. Int J Adhes Adhes 45:69–76

Krüeger R, O'Brien TK (2001) A shell/3D modelling technique for the analysis of delaminated composite laminates. Compos A 32:25–44

Lai YH, Rakestraw MD, Dillards DA (1996) The cracked lap shear specimen revisited—a closed form solution. Int J Solids Struct 33:1725–1743

Nassar SA, Mao J, Yang X (2012) A damage model for adhesively bonded single-lap thick composite joints. ASME Trans J Eng Mater Technol. doi:10.1115/1.4006821

Nguyen VP, Kerfriden P, Bordas SPA, Rabczuk T (2014a) Isogeometric analysis suitable trivariate NURBS representation of composite panels with a new offset algorithm. Comput Aided Des 55:49–63

Nguyen VP, Kerfriden P, Bordas S (2014b) Two- and three-dimensional isogeometric cohesive elements for composite delamination analysis. Compos B Eng 60:193–212

Pagano NJ, Pipes RB (1973) Some observations on the inter laminar strength of composite laminates. Int J Mech Sci 8:679–686

Panigrahi SK (2013) Structural design of single lap joints with laminated FRP composite adherends. Compos Part B 51:112–120

Panigrahi SK, Pradhan B (2007) Three dimensional failure analysis and damage propagation behavior of adhesively bonded single lap joints in laminated FRP composites. J Reinf Plast Compos 21:183–200

Panigrahi SK, Pradhan B (2009) Through-the-width delamination damage propagation characteristics in single-lap laminated FRP composite joints. Int J Adhes Adhes 29:114–124

Parida SK, Pradhan AK (2014) 3D finite element analysis of stress distributions and strain energy release rates for adhesive bonded flat composite lap shear joints having pre-existing delaminations. J Mech Sci Technol 20:481–488

Pradhan B (1982) Effect of width and axial to transverse elastic stiffness ratio on SCF in uniaxially loaded FRP composite plates containing circular holes. Fibre Sci Technol 17:245–254

Pradhan AK, Parida SK (2012) 3D FE delamination induced damage analyses of lap shear joints made with curved laminated FRP composite panels. J Adhes Sci Technol 27:1104–1121

Raju IS, Crews JH, Aminpour MA (1988) Convergence of strain energy release rate components for edge-delaminated composite laminates. Eng Fract Mech 30:383–396

Riccio A, Raimondo A, Scaramuzzino F (2015) A robust numerical approach for the simulation of skin-stringer debonding growth in stiffened composite panels under compression. Compos B Eng 71:131–142

Riccio A, Damiano M, Raimondo A, Di Felice G, Sellitto A (2016) A fast numerical procedure for the simulation of inter-laminar damage growth in stiffened composite panels. Compos Struct 145:203–216

Rice JR (1988) Elastic fracture mechanics concepts for interfacial cracks. ASME Trans J Appl Mech 55:98–103

Rybicki EF, Kanninen MF (1977) A finite element calculation of stress intensity factors by a modified crack closure integral. Eng Fract Mech 9:931–938

Tay TE (2003) Characterization and analysis of delamination fracture in composites: an overview of developments from 1990 to 2001. Appl Mech Rev 56:1–32

Tay TE, Shen F, Lee KH, Scaglione A, Sciuva MD (1999) Mesh design in finite element analysis of post-buckled delamination in composite laminates. Compos Struct 47:603–611

Tian Y, Fu Y (2011) Modelling of composite laminated plates with interfacial damage evolution. Int J Damage Mech 20:369–399

Tong L (1996) Bond strength for adhesive-bonded single lap joints. Acta Mech 117:101–113

Tsai MY, Oplinger DW, Morton J (1998) Improved theoretical solutions for adhesive lap joints. Int J Solids Struct 35:1163–1185

Volkersen O (1938) Die nietkraftverteilung in zugbeanspruchten nietverbindungen mit konstanten laschenquerschnitten. Luftfahrtforschung 15:41–47

Wang JT, Raju IS (1996) Strain energy release rate formulae for skin-stiffener debond modelled with plate elements. Eng Fract Mech 54:211–228

Wang H, Vu-Khanh T (1995) Fracture mechanics and mechanisms of impact-induced delamination in laminated composites. J Compos Mater 29:156–178

Yang C, Tomblin JS, Guan Z (2003) Analytical modeling of ASTM lap shear adhesive specimens. Report, U.S. Department of Transportation Federal Aviation Administration Office of Aviation Research, Washington, DC, 20591, DOT/FAA/AR-02/130. http://www.tc.faa.gov/its/worldpac/techrpt/ar02-130.pdf. Accessed 15 Mar 2016

Zhang BM, Zhao L (2012) Progressive damage and failure modelling in fiber-reinforced laminated composites containing a hole. Int J Damage Mech 21:892–911